Investigating Molecular Junctions Based on Mixed SAMs to Understand the Impact of Intermolecular, Intra-SAM Interactions on Transport

Jiajun Feng,[§] Ioan Bâldea,[†,*] Jiajie Gao,[§] Gookyeong Jeong,[‡] C. Daniel Frisbie,[‡,*] and Zuoti Xie[§,∥,*]

[§] Department of Materials Science and Engineering, Guangdong Provincial Key Laboratory of Materials and Technologies for Energy Conversion (MATEC), Guangdong Technion-Israel Institute of Technology, 241 Daxue Road, Shantou, Guangdong, 515063, China

[†] Theoretical Chemistry, Heidelberg University, Im Neuenheimer Feld 229, D-69120 Heidelberg, Germany

[‡] Department of Chemical Engineering and Materials Science and Department of Chemistry, University of Minnesota, Minneapolis, Minnesota 55455, United States

[∥] Quantum Science Center of Guangdong-Hong Kong-Macao Greater Bay Area (Guangdong), Shenzhen-Hong Kong International Science and Technology Park, NO.3 Binglang Road, Futian District, Shenzhen, Guangdong, 518000, China

*To whom correspondence should be addressed
E-mail: ioan.baldea@pci.uni-heidelberg.de; frisbie@umn.edu, zuoti.xie@gtiit.edu.cn

Abstract

To interrogate the importance of intermolecular interactions on charge transport at the nanoscale, we investigate molecular tunnel junctions based on mixed self-assembled monolayers (SAMs) of 1-alkyl (CnT) thiols and their fluorinated counterparts (F-CnT) that have substantially different tunneling conductances. Experiments on mixed CnT_{1-x}:F-CnT_x SAMs between Au contacts reveal a strongly nonlinear (exponential) dependence of the tunneling conductance G on composition x, a behavior that is tempting to assign to the strong impact of intra-SAM intermolecular interactions. However, analysis suggests that the exponential dependence of G on x does not arise from intra-SAM intermolecular interactions, but instead emerges from the work function modification of the Au electrode which varies linearly with x.

KEYWORDS: molecular electronics, tunnel junction, conducting probe AFM (CP-AFM), mixed SAM, intermolecular interactions, work function.

With a few exceptions (*e.g.*, mechanically controlled break junctions, MC-BJ[1–9] or junctions with single layer graphene[10,11]), molecular tunnel junctions are fabricated using a self-assembled monolayer (SAM) adsorbed on a substrate electrode.[12-16] Therefore, whether the current through a molecule is affected by interactions with the surrounding molecules is a legitimate question not only for junctions possessing a top electrode having an area ranging from a few tens on nm^2 (the case of conducting probe atomic force microscopy (CP-AFM) junctions[17-21]) to hundreds of um^2 (the case of large area eutectic GaIn (EGaIn)-based junctions[22-26]), but also for STM-BJ single molecule setups.[27-31]

In this work, we address this issue by fabricating CP-AFM tunnel junctions using mixed SAMs containing[32-34] two types of molecules, alkyl monothiols (CnT) and their fluorinated counterparts (F-CnT), defined as $-S-(CH_2)_{n-1}CH_3$ for CnT and $-S-(CH_2)_2(CF_2)_{n-3}CF_3$ for F-CnT, with n representing chain lengths of 6, 8, and 10, **Figure 1**. The composition of the mixed SAM is given by CnT_{1-x}:F-CnT_x where x is the fraction of F-CnT on the surface.

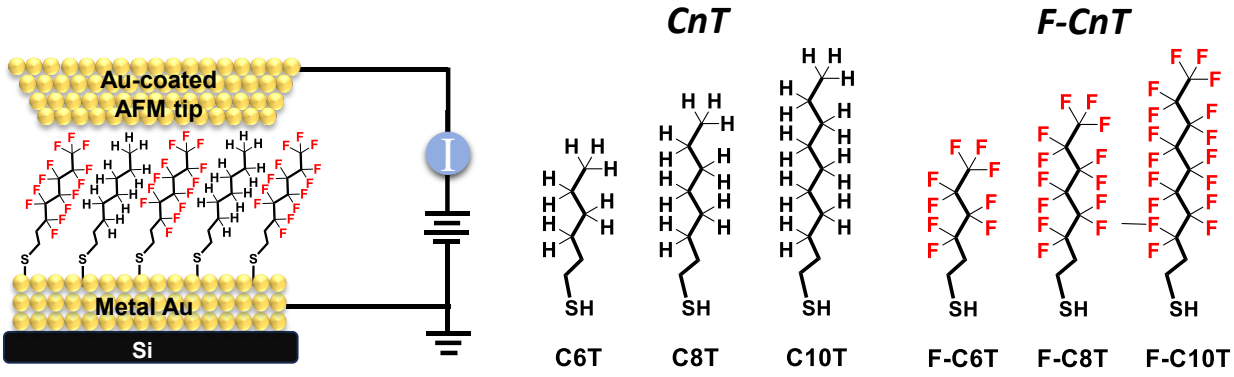

Figure 1. Schematic representation of the CP-AFM setup: a gold-coated AFM tip touches a mixed SAM of alkyl and fluoroalkyl monothiols (CnT, F-CnT, n=6, 8, 10) absorbed on a gold-coated substrate.

With these mixed SAM junctions our goal is to check is whether the conductances of the two molecular species are additive (two independent conductors in parallel) or not, *i.e.*,

$$G(x) \overset{?}{=} (1-x)G_{CnT} + xG_{F-CnT} \quad (1)$$

The rationale here is that linear dependence of G on x as suggested by eq (1) could indicate that mixing is "ideal" (no intermolecular interactions), *i.e.*, that the conductances of the two molecules simply add, whereas non-linear dependence on x (contrary to eq (1)) could indicate non-ideal mixing and a significant role for intermolecular effects. Equations like eq (1) are often used for predicting properties of mixtures in the ideal limit (*e.g.*, vapor pressures) and are generally referred to as "mixing rules".[35-37]

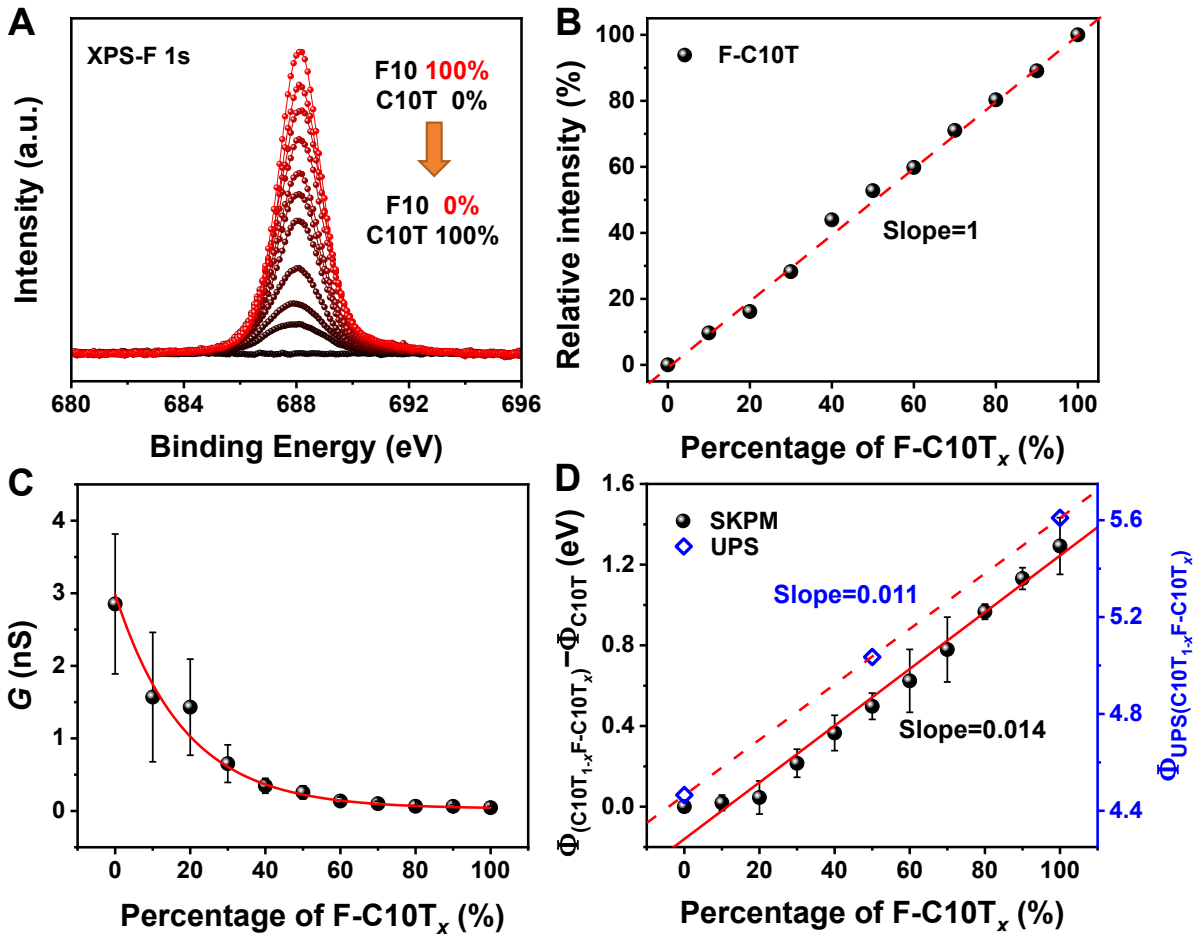

Figure 2. (A) F 1s core-level XPS spectra of C10T$_{1-x}$:F-C10T$_x$ mixed SAMs as a function of F-C10T in the deposition solution. (B) The intensity of the F 1s signal as a function of the percentage of F-C10T in solution indicating that surface concentration maps linearly to the deposition solution concentration. (C) Junction conductance G vs composition in the mixed SAM. (D) The change of the work function as a function of the percentage of F-C10T.

Prior to conducting measurements on the F-CnT and CnT mixed SAM samples, X-ray photoelectron spectroscopy (XPS) was employed to characterize the relative changes in the F 1s signal of the mixed samples, thereby confirming the relative surface concentration *x* of F-CnT, **Figure 2A**. An example of this analysis is shown in **Figure 2B** where a linear increase in the relative intensity of the F 1s core-level signal is observed from the SAMs as a function of F-C10T concentration in the deposition solution. The slope of this graph is 1 indicating that the surface concentration maps linearly to the deposition solution concentration.[33]

A key result is shown in **Figure 2C**: low bias junction conductance exhibits a strong downward trend with increasing F-C10T percentages. **Figure 2D** extends this analysis by comparing the changes in work function measured by both scanning Kelvin probe force microscopy (SKPM) and ultra-violet photoelectron spectroscopy (UPS), revealing a consistent increase in the work function difference with a higher content of F-C10T. SKPM and UPS measurement details are shown in **Figures S2-6**.

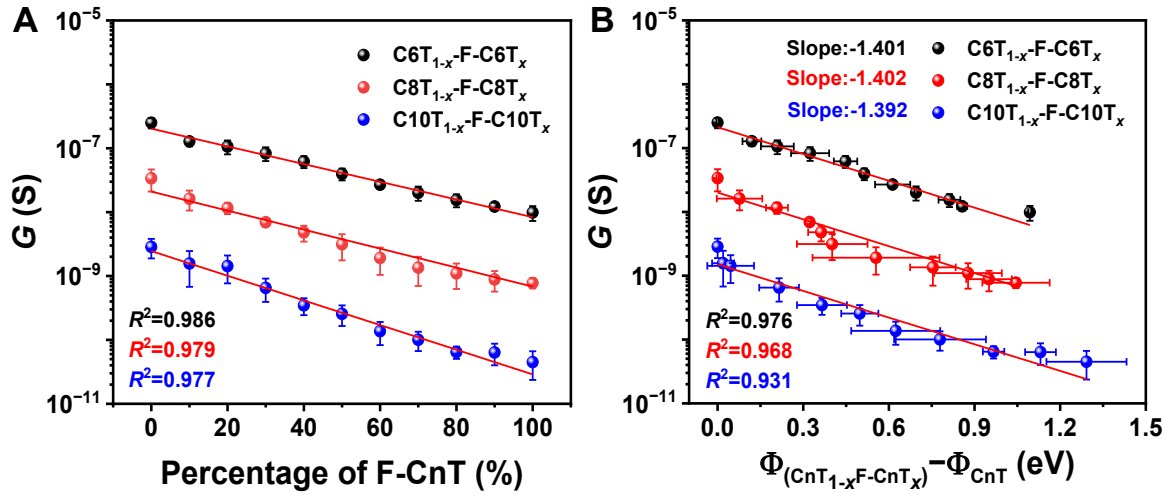

Figure 3. Semilog plot of low bias conductance *G* of the mixed $CnT_{1-x}F\text{-}CnT_x$ SAMs as a function of (A) percentage of F-CnT and (B) difference of work function between $CnT_{1-x}F\text{-}CnT_x$/Au and CnT/Au.

Our data for the low bias conductance $G(x)$ measured for mixed CnT_{1-x}:F-CnT_x SAMs are at odds with the linear dependence on composition expressed by eq (1). More precisely, the strongly nonlinear dependence of G on x found in the experiment, **Figure 2C**, turns out to be exponential, as shown in **Figures 3A, S7C** and **S8C**. That is,

$$G(x) \propto \exp(ax) \tag{2}$$

where a is a constant (quantity independent of x).

In the spirit that motivated the present investigation, it would be tempting to conclude that the experimental finding expressed by eq (2) constitutes exemplary evidence for the importance of intermolecular interactions within the SAM. However, eq (1) misses an important effect, namely, the relationship between the conductance G of the junction and the electrode work function change $\Delta\Phi$ caused by the adsorbed SAM, **Figure 3B**.[38–40]

This is an important point because what makes the F-CnT junctions different from the CnT junctions is not only their conductance G but also the SAM-driven change in the electrode work function:

$$\Delta\Phi = \Phi_{SAM/Au} - \Phi_{Au}$$

Gold electrodes coated with F-CnT SAMs have work functions larger by about 1 eV than gold electrodes coated with CnT, Table 1. These values of $\Delta\Phi$ are comparable with the work function changes reported previously for various molecular species on metals.[38,41,42] Importantly, irrespective of whether the molecules employed were aromatic[38,41] or aliphatic,[42] those studies invariably reported a strong exponential dependence of G on $\Delta\Phi$:

$$G \propto \exp(b\Delta\Phi) \tag{3}$$

indicating thereby the general character of this dependence. Above, b is a constant (quantity independent of $\Delta\Phi$). Further, we note that eq (3) was a key ingredient in successfully estimating

the number of current carrying molecules in large area junctions with eutectic Ga-In top electrodes.[43,44]

Table 1. Low-bias conductance G and work functions $\Phi_{SAM/Au}$ measured for gold electrodes coated with alkyl thiols (CnT) and their fluorinated counterparts (F-CnT) by UPS (see Figure S9 in the SI).

Molecule	G (S)	Φ(eV)
C6T	3.34×10^{-7}	4.68
F-C6T	9.86×10^{-9}	5.37
C8T	3.18×10^{-8}	4.70
F-C8T	7.78×10^{-10}	5.45
C10T	3.26×10^{-9}	4.46
F-C10T	9.46×10^{-11}	5.61

Returning to eq (1) with this in mind, one can easily realize that this linear equation would hold only if the gold substrate coated with mixed SAMs had locally inhomogeneous work functions switching between two distinct values, as schematically depicted by the cartoon of **Figure 4B**, i.e., one value $\Phi_{CnT/Au}$ at the sites in contact to CnT molecules and another value $\Phi_{F\text{-}CnT/Au}$ at the sites in contact to F-CnT molecules. Here, $\Phi_{CnT/Au}$ and $\Phi_{F\text{-}CnT/Au}$ represent work functions of homogeneous SAMs merely consisting of CnT and F-CnT molecules, respectively, **Figure 4A**.

Transposing the idea underlying **Figure 4B** to the two-dimensional SAM geometry, eq (1) would hold only if the work function map of a gold electrode coated with a mixed CnT_{1-x}:F-CnT_x SAM would be a black and white checkered table comprising a fraction $1-x$ of black squares and a fraction x of white squares wherein the values assigned are $\Phi_{CnT/Au}$ and $\Phi_{F\text{-}CnT/Au}$, respectively.

The foregoing picture (**Figure 4A**) might apply to mixed SAMs formed on hypothetical substrates possessing localized electrons (i.e., insulators) but not to metal substrates. Given the highly delocalized metal electrons over distances longer than the intermolecular spacing (~ 5Å) characterizing our closely packed alkane-based SAMs with coverages $\Sigma \simeq 3.5$ molecules/nm^2

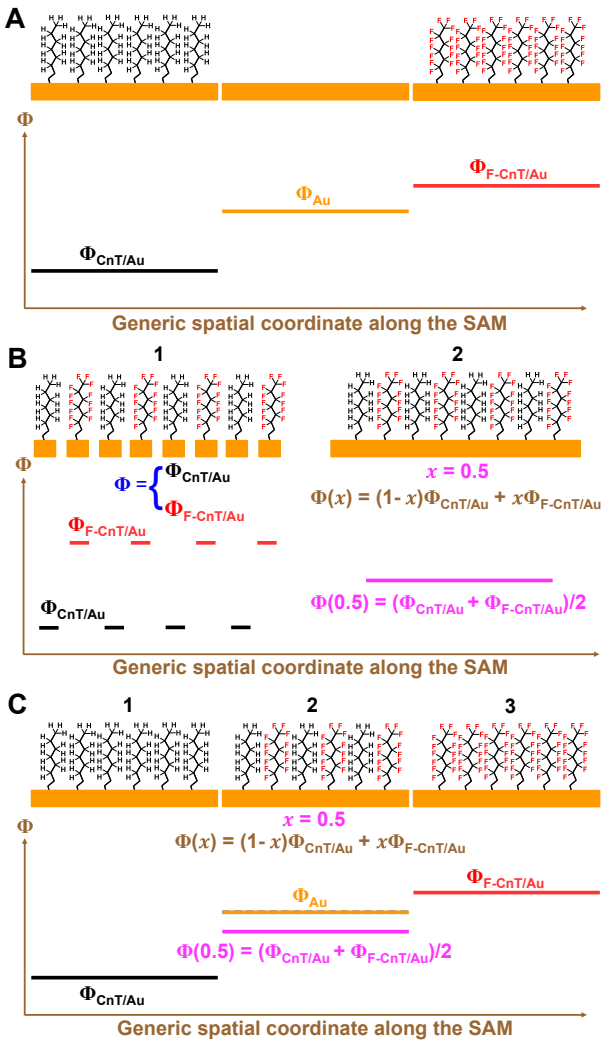

Figure 4. Schematic representation of the work function of (A) pure SAMs and (B) mixed $CnT_{1-x}F\text{-}CnT_x$ SAMs wherein closely packed molecules give rise to an averaged, (C) nearly position-independent work function at the interface. Panel A visualizes the fact that homogeneous SAMs of CnT (left) and F-CnT (right) change the work function of the bare metal (Φ_{Au}, middle) to significantly different values ($\Phi_{CnT/Au} \neq \Phi_{F\text{-}CnT/Au}$). Panel B simulates a SAM wherein CnT and F-CnT molecules alternate (concentration x=0.5) in two different situations (cases 1 and 2). Case 1 depicts the SAM adsorbed on a hypothetical substrate whose electrons are localized. This hypothetical substrate is depicted as an interrupted orange bar in panel A. On the small orange portions that mimic single adsorption sites, the local work function is nonhomogeneous; it switches between the values $\Phi_{CnT/Au}$ and $\Phi_{F\text{-}CnT/Au}$ depending on whether the adsorbed molecule is CnT or F-CnT. If this (black-white checkered table) picture held, the left and right hand sides of eq (1) would be equal. Case 2 mimics a real metallic substrate. Because its electrons are delocalized (non-interrupted orange bar in panel B), the work function is homogeneous (nearly position independent). Its value $\Phi(x)$ is determined by the average of the individual values $\Phi_{CnT/Au}$ and $\Phi_{F\text{-}CnT/Au}$ weighted by the corresponding concentrations and varies between the values $\Phi(x{=}0) = \Phi_{CnT/Au}$ and $\Phi(x{=}1) = \Phi_{F\text{-}CnT/Au}$ (panel C). At equal concentrations (x=0.5, case 2 in panel B, same as case 2 in panel C), the homogeneous (position-independent) value $\Phi(x{=}0.5)$ represents the arithmetic average of $\Phi_{CnT/Au}$ (case 1 in panel C) and $\Phi_{F\text{-}CnT/Au}$ (case 3 in panel C).

measured via Rutherford backscattering (RBS) and nuclear reaction analysis (NRA),[45] one can rather expect a spatially uniform work function expressed as a weighted average (**Figure 4C**)

$$\Delta\Phi(x) = (1 - x)\Delta\Phi_{CnT} + x\Delta\Phi_{F-CnT} \quad (4)$$

This weighted average is precisely what we observe by SKPM in Figure **2D**. UPS measurements, which cannot achieve (sub)nanometer spatial resolution, confirmed the linear dependence of $\Delta\Phi$ on composition expressed by eq (4) (**Figures 2D, S7D and S8D**). Thus, our results show that the linear mixing rule for conductance given by eq (1) does not hold (see Figure **2C**) but rather that linear mixing applies to the work function, as captured by eq (4) and shown in Figure **2D**.

Combining eqs (2) and (4) — that is, our experimental findings — we arrive at:

$$G(x) \propto \exp\left[\frac{a}{\Delta\Phi_{F-CnT} - \Delta\Phi_{CnT}}\Delta\Phi(x)\right]$$

which is in the form of eq (3), thereby in favor of a general physics underlying that equation. Alternatively, the insertion of eq (4) into eq (3) yields

$$\mathrm{G}(x) \propto \exp\left[b(\Delta\Phi_{F-CnT} - \Delta\Phi_{CnT})x\right] \quad (5)$$

To better understand the generality of the above formula, we emphasize that it is "free" of any extra (theoretical) assumption: eq (3) and eq (4) are experimental findings; eq (3) expresses a general relationship between conductance and SAM-driven electrode work function observed by molecular junctions fabricated with qualitatively different types of molecular species and metal electrodes.[38,41,42]

Eq (5) — which is exactly of the form found in the experiment ($a \equiv b(\Delta\Phi_{F-CnT} - \Delta\Phi_{CnT})$ in eq (2) — is our most important result. Along with specific arguments based on quantum chemical calculations (see Section "Quantum Chemical Calculations" and Figure **S10** in the SI), eq (5) does *not* substantiate an important impact of intra-SAM intermolecular interactions on

tunneling transport. The exponential dependence of G on x can be explained simply by the work function change with x. Figure **S10** in the SI and associated discussion show that in fact there is very little HOMO-HOMO overlap in this system, consistent with this interpretation.

Putting in more physical terms, the elementary transport process through a CnT molecule (to be more specific, a hole tunneling mediated by the CnT's HOMO[42]) occurs at a rate (in units of $\hbar = 1$) $\Gamma_{CnT} = \Gamma_{CnT}(x) \propto \sqrt{G_{CnT}(x)}$ which is modulated (i) by the work function change $\Delta\Phi(x)$ due to the mixed SAM and (ii) not by the work function change $\Delta\Phi_{(CnT)}$ due to a pure CnT SAM adsorbed on gold. Likewise, the elementary transport process through a F-CnT molecule (to be more specific, a hole tunneling mediated by F-CnT's HOMO[42]) occurs at a rate $\Gamma_{F-CnT} = \Gamma_{F-CnT}(x) \propto \sqrt{G_{F-CnT}(x)}$, (*cf.*, *e.g.*, eq (3) in ref. 42) which is modulated (i) by the work function change $\Delta\Phi(x)$ due to the mixed SAM and (ii) not by the work function change $\Delta\Phi_{(F\text{-}CnT)}$ due to a pure F-CnT SAM on gold. Experiments say that the conductance varies exponentially with x (eq (2) and Figure 2C). If clause (ii) is applied, the conductance would vary linearly with x (eq (1)), a behavior that naive intuition might expect but the experiment rejects. Currents I measured at larger biases behave similarly to the low bias conductance G (*cf.* **Figure S11**). The reason is that the expressions for both G and I contain the same factor of Γ^2 (*cf.* eq (4) of ref. 43 and eq (7) of ref. 44).

So, paradoxically, it is just the exponential dependence of G on x that initially seemed to be evidence of important intra-SAM interactions that has eventually led to the conclusion that the contrary is true. That is, for the $CnT_{1\text{-}x}$:F-CnT_x mixed SAM system, intermolecular interactions do not appear to have a significant impact on the measured tunneling conductance. Future measurements on other mixed SAM systems, such as those based on aromatic molecules, will be used to assess the generality of this conclusion.

Before ending, we emphasize that, in order to clearly discriminate between linear dependence (eq (1)) and exponential dependence (eq (2)) of conductance, the two molecular species of the mixed SAM were chosen such that junctions made of pure SAMs (x = 0, pure CnT versus x = 1, pure F-CnT) have significantly different conductances ($G_{CnT}/G_{F-CnT}\sim10^2$, *cf.* Table 1).

Experimental Method

Materials. The materials used in this experiment included highly pure gold nuggets (99.999%), silver pellets (99.99%), platinum targets (99.99%), titanium (99.99%), and chromium evaporation rods, all supplied by Kurt J. Lesker Co. Contact mode AFM silicon nitride probes were provided by Bruker AFM Probes. The alkanethiols and fully fluorinated alkanethiols used, with varying chain lengths, included 1-hexanethiol (C6T, 99%), 1-octanethiol (C8T, 98.5%), and 1-decanethiol (C10T, 99%), along with their fluorinated derivatives, 13-fluoro-1-octanethiol (F-C8T, 98%) and 17-fluoro-1-decanethiol (F-C10T, 98%), all of which were acquired from Sigma-Aldrich. Nonafluoro-1-hexanethiol (F-C6T, 98%) was obtained from HEOWNS.

Sample Preparation. Mixed $CnT_{1-x}F\text{-}CnT_x$ solutions were prepared by adding CnT and F-CnT to 10 ml of ethanol in varying volume ratios, ensuring the total addition was 3 microliters for both CnT and F-CnT in the mixture. Template-stripped flat metal substrates were then immersed individually in these solutions with different proportions for 20 hours.[46] Following the immersion, substrates were thoroughly rinsed with ethanol and dried under nitrogen flow. After these preparation steps, the samples were ready for subsequent measurement and analysis.

Ellipsometry and Scanning Kelvin Probe Microscopy (SKPM) Measurements. The thicknesses of CnT and F-CnT films for SAMs were measured by ellipsometry, as shown in

Figure S1. SKPM was used to determine the relative difference in work function (ΔΦ) with different SAMs adsorbed on the metal surface. The surface contact potential of the samples was measured using the same instrument employed for *I-V* characterization. The AFM instrument was located in an Ar-filled glove box (H_2O, O_2 <0.1 ppm). The typical surface potential images and histograms are presented in **Figure S2**.

XPS and UPS Measurements. The X-ray photoelectron spectroscopy (XPS) measurements were conducted on a PHI VersaProbe III XPS system (ULVAC-PHI) using a monochromatic Al K_α X-ray source (1486.6 eV). Relevant results are presented in **Figures S6(A, B)** and **S7(A, B)**.The X-ray spot size was 200 micrometers, with a power of 25 watts at 15 kilovolts. F 1s core-level spectra were collected using 112 eV pass energy, a time per step of 10 ms, and 30 cycles. UPS measurements were performed in the same system as for XPS, utilizing a He I light source (21.2 eV). UPS spectra were collected using 1.3 eV pass energy, 0.05 eV per step, and 20 seconds per step, with the takeoff angle set to 45°. In the UPS acquisition, a voltage of -5 V was applied to the sample to obtain the secondary electron cutoff.

Transport Measurements. The experimental setup for transport measurements was similar to that in our previous work.[46] CP-AFM-based molecular junctions were constructed by mounting the substrates in the AFM and approaching the SAM with metal-coated tips under an ~ +1 nN applied compressive load. Voltage was applied spanning ±1.5 V for junctions. The slope of the low-bias I−V characteristic (linear portion within the bias range of ±0.1 V) was employed to extract (low-bias) junction conductance *G*.

Quantum Chemical Calculations. Elaborate ab initio chemical calculations based on outer valence Green's functions (OVGF)[47,48] similar to those of our previous studies[46,49,50] were carried

out to microscopically interrogate the impact of intra-SAM intermolecular interactions on the HOMO energies. Natural orbital expansions of the one-particle reduced density matrix allow the adequate determination of the relevant hole (HOMO) spatial distributions (Figure S10 in the SI), like those of our earlier work.[51,52] To this aim, we used the GAUSSIAN 16[53] package.

Associated Content

Conflicts of interest: The authors declare no competing financial interests.

Acknowledgement. Z.X. acknowledges primary financial support from the National Key R&D Program of China (2023YFA1407100), the National Natural Science Foundation of China (22373026), and the Guangdong Science and Technology Department (2021B0301030005, 2022A1515011843, GDZX2304005, 2021QN02X538 and STKJ2023072). I.B. acknowledges computational support by the state of Baden-Württemberg through bwHPC and the German Research Foundation through Grant No. INST 40/575-1 FUGG (bwUniCluster 2.0, bwForCluster/HELIX, and JUSTUS 2.0 cluster). C.D.F thanks the US National Science Foundation (NSF) for financial support through CHE-2304763.

Supporting Information Available. Experimental and theoretical details, supplementary tables and figures. This material is available free of charge *via* the Internet at http://pubs.acs.org/.

References

(1) Reed, M. A.; Zhou, C.; Muller, C. J.; Burgin, T. P.; Tour, J. M. Conductance of a Molecular Junction. *Science* **1997**, *278*, 252–254.

(2) Reddy, H.; Wang, K.; Kudyshev, Z.; Zhu, L.; Yan, S.; Vezzoli, A.; Higgins, S. J.; Gavini, V.; Boltasseva, A.; Reddy, P.; Shalaev, V. M.; Meyhofer, E. Determining Plasmonic Hot-Carrier Energy Distributions via Single-Molecule Transport Measurements. *Science* **2020**, *369*, 423–426.

(3) Guo, C.; Wang, K.; Zerah-Harush, E.; Hamill, J.; Wang, B.; Dubi, Y.; Xu, B. Molecular Rectifier Composed of DNA with High Rectification Ratio Enabled by Intercalation. *Nat. Chem.* **2016**, *8*, 484–490.

(4) Mayor, M.; Von Hänisch, C.; Weber, H. B.; Reichert, J.; Beckmann, D. Atrans-Platinum (II) Complex as a Single-Molecule Insulator. *Angew. Chem. Int. Ed.* **2002**, *41*, 1183–1186.

(5) Lörtscher, E.; Weber, H. B.; Riel, H. Statistical Approach to Investigating Transport through Single Molecules. *Phys. Rev. Lett.* **2007**, *98*, 176807.

(6) Martin, C. A.; Smit, R. H. M.; Van Der Zant, H. S. J.; Van Ruitenbeek, J. M. A Nanoelectromechanical Single-Atom Switch. *Nano Lett.* **2009**, *9*, 2940–2945.

(7) Zang, Y.; Pinkard, A.; Liu, Z.-F.; Neaton, J. B.; Steigerwald, M. L.; Roy, X.; Venkataraman, L. Electronically Transparent Au–N Bonds for Molecular Junctions. *J. Am. Chem. Soc.* **2017**, *139*, 14845–14848.

(8) Li, X.; Zheng, Y.; Zhou, Y.; Zhu, Z.; Wu, J.; Ge, W.; Zhang, Y.; Ye, Y.; Chen, L.; Shi, J.; Liu, J.; Bai, J.; Liu, Z.; Hong, W. Supramolecular Transistors with Quantum Interference Effect. *J. Am. Chem. Soc.* **2023**, *145*, 21679–21686.

(9) Jeong, H.; Li, H. B.; Domulevicz, L.; Hihath, J. An On-Chip Break Junction System for Combined Single-Molecule Conductance and Raman Spectroscopies. *Adv. Funct. Mater.* **2020**, *30*, 2000615.
(10) Yang, C.; Yang, C.; Guo, Y.; Feng, J.; Guo, X. Graphene–Molecule–Graphene Single-Molecule Junctions to Detect Electronic Reactions at the Molecular Scale. *Nat. Protoc.* **2023**, *18*, 1958–1978.
(11) Bâldea, I.; Chen, Y.; Zhang, M.; Xin, N.; Feng, Y.; Feng, J.; Jia, C.; Guo, X.; Xie, Z. Breakdown of Ohm's Law in Molecular Junctions with Electrodes of Single-Layer Graphene. *J. Phys. Chem. Lett.* **2024**, *15*, 3267–3275.
(12) Love, J. C.; Estroff, L. A.; Kriebel, J. K.; Nuzzo, R. G.; Whitesides, G. M. Self-Assembled Monolayers of Thiolates on Metals as a Form of Nanotechnology. *Chem. Rev.* **2005**, *105*, 1103–1170.
(13) Du, W.; Chen, X.; Wang, T.; Lin, Q.; Nijhuis, C. A. Tuning Overbias Plasmon Energy and Intensity in Molecular Plasmonic Tunneling Junctions by Atomic Polarizability. *J. Am. Chem. Soc.* **2024**, *146*, 21642–21650.
(14) Kumar, S.; Soni, S.; Danowski, W.; van Beek, C. L. F.; Feringa, B. L.; Rudolf, P.; Chiechi, R. C. Correlating the Influence of Disulfides in Monolayers across Photoelectron Spectroscopy Wettability and Tunneling Charge-Transport. *J. Am. Chem. Soc.* **2020**, *142*, 15075–15083.
(15) Kong, G. D.; Byeon, S. E.; Jang, J.; Kim, J. W.; Yoon, H. J. Electronic Mechanism of In Situ Inversion of Rectification Polarity in Supramolecular Engineered Monolayer. *J. Am. Chem. Soc.* **2022**, *144*, 7966–7971.
(16) Cho, K.; Pak, J.; Chung, S.; Lee, T. Recent Advances in Interface Engineering of Transition-Metal Dichalcogenides with Organic Molecules and Polymers. *ACS Nano* **2019**, *13*, 9713–9734.
(17) Wold, D. J.; Frisbie, C. D. Formation of Metal−Molecule−Metal Tunnel Junctions: Microcontacts to Alkanethiol Monolayers with a Conducting AFM Tip. *J. Am. Chem. Soc.* **2000**, *122*, 2970–2971.
(18) Xie, Z.; Bâldea, I.; Demissie, A. T.; Smith, C. E.; Wu, Y.; Haugstad, G.; Frisbie, C. D. Exceptionally Small Statistical Variations in the Transport Properties of Metal–Molecule–Metal Junctions Composed of 80 Oligophenylene Dithiol Molecules. *J. Am. Chem. Soc.* **2017**, *139*, 5696–5699.
(19) Nguyen, A. T.; Louis-Goff, T.; Ortiz-Garcia, J. J.; Pham, T. K. N.; Quardokus, R. C.; Lee, E.-C.; Brown, J. J.; Hyvl, J.; Lee, W. Cluster Formation of Self-Assembled Triarylbismuthanes and Charge Transport Characterizations of Gold–Triarylbismuthane–Gold Junctions. *ACS Appl. Mater. Interfaces* **2024**, *16*, 38669–38678.
(20) Parker, C. R.; Leary, E.; Frisenda, R.; Wei, Z.; Jennum, K. S.; Glibstrup, E.; Abrahamsen, P. B.; Santella, M.; Christensen, M. A.; Della Pia, E. A.; Li, T.; Gonzalez, M. T.; Jiang, X.; Morsing, T. J.; Rubio-Bollinger, G.; Laursen, B. W.; Nørgaard, K.; Van Der Zant, H.; Agrait, N.; Nielsen, M. B. A Comprehensive Study of Extended Tetrathiafulvalene Cruciform Molecules for Molecular Electronics: Synthesis and Electrical Transport Measurements. *J. Am. Chem. Soc.* **2014**, *136*, 16497–16507.
(21) Ditzler, L. R.; Karunatilaka, C.; Donuru, V. R.; Liu, H. Y.; Tivanski, A. V. Electromechanical Properties of Self-Assembled Monolayers of Tetrathiafulvalene Derivatives Studied by Conducting Probe Atomic Force Microscopy. *J. Phys. Chem. C* **2010**, *114*, 4429–4435.
(22) Bowers, C. M.; Liao, K.-C.; Zaba, T.; Rappoport, D.; Baghbanzadeh, M.; Breiten, B.; Krzykawska, A.; Cyganik, P.; Whitesides, G. M. Characterizing the Metal–SAM Interface in Tunneling Junctions. *ACS Nano* **2015**, *9*, 1471–1477.
(23) Fracasso, D. Self-Assembled Monolayers of Terminal Acetylenes as Replacements for Thiols in Bottom-up Tunneling Junctions. *RSC Adv.* **2014**, *4*, 56026–56030.
(24) Kong, G. D.; Jin, J.; Thuo, M.; Song, H.; Joung, J. F.; Park, S.; Yoon, H. J. Elucidating the Role of Molecule–Electrode Interfacial Defects in Charge Tunneling Characteristics of Large-Area Junctions. *J. Am. Chem. Soc.* **2018**, *140*, 12303–12307.
(25) Kong, G. D.; Kim, M.; Cho, S. J.; Yoon, H. J. Gradients of Rectification: Tuning Molecular Electronic Devices by the Controlled Use of Different-sized Diluents in Heterogeneous Self-assembled Monolayers. *Angew. Chem. Int. Ed.* **2016**, *55*, 10307–10311.
(26) Chen, J.; Giroux, T. J.; Nguyen, Y.; Kadoma, A. A.; Chang, B. S.; VanVeller, B.; Thuo, M. M. Understanding Interface (Odd–Even) Effects in Charge Tunneling Using a Polished EGaIn Electrode. *Phys. Chem. Chem. Phys.* **2018**, *20*, 4864–4878.
(27) Xu, B.; Tao, N. J. Measurement of Single-Molecule Resistance by Repeated Formation of Molecular Junctions. *Science* **2003**, *301*, 1221–1223.

(28) Guo, S.; Hihath, J.; Díez-Pérez, I.; Tao, N. Measurement and Statistical Analysis of Single-Molecule Current–Voltage Characteristics, Transition Voltage Spectroscopy, and Tunneling Barrier Height. *J. Am. Chem. Soc.* **2011**, *133*, 19189–19197.
(29) Fang, C.; Almughathawi, R.; Wu, Q.; Cao, W.; Chen, H.; Hou, S.; Gu, Y.; Zhang, H.; Zhao, Y.; Zheng, J.; Li, G.; Shi, J.; Liu, J.; Mao, B.-W.; Liu, Z.; Lambert, C. J.; Hong, W. Intermolecular Coupling Enhanced Thermopower in Single-Molecule Diketopyrrolopyrrole Junctions. *Natl. Sci. Open* **2023**, *2*, 20220039.
(30) Zhang, C.; Cheng, J.; Wu, Q.; Hou, S.; Feng, S.; Jiang, B.; Lambert, C. J.; Gao, X.; Li, Y.; Li, J. Enhanced π–π Stacking between Dipole-Bearing Single Molecules Revealed by Conductance Measurement. *J. Am. Chem. Soc.* **2023**, *145*, 1617–1630.
(31) Frisenda, R.; Janssen, V. A. E. C.; Grozema, F. C.; Van Der Zant, H. S. J.; Renaud, N. Mechanically Controlled Quantum Interference in Individual π-Stacked Dimers. *Nat. Chem.* **2016**, *8*, 1099–1104.
(32) Laibinis, P. E.; Fox, M. A.; Folkers, J. P.; Whitesides, G. M. Comparisons of Self-Assembled Monolayers on Silver and Gold: Mixed Monolayers Derived from $HS(CH_2)_{21}X$ and $HS(CH_2)_{10}Y$ (X, Y = CH_3, CH_2OH) Have Similar Properties. *Langmuir* **1991**, *7*, 3167–3173.
(33) Folkers, J. P.; Laibinis, P. E.; Whitesides, G. M.; Deutch, J. Phase Behavior of Two-Component Self-Assembled Monolayers of Alkanethiolates on Gold. *J. Phys. Chem.* **1994**, *98*, 563–571.
(34) Chapman, R. G.; Ostuni, E.; Yan, L.; Whitesides, G. M. Preparation of Mixed Self-Assembled Monolayers (SAMs) That Resist Adsorption of Proteins Using the Reaction of Amines with a SAM That Presents Interchain Carboxylic Anhydride Groups. *Langmuir* **2000**, *16*, 6927–6936.
(35) Janzen, J. Elastic Moduli of Semicrystalline Polyethylenes Compared with Theoretical Micromechanical Models for Composites. *Polym. Eng. & Sci* **1992**, *32*, 1242–1254.
(36) Hou, S.-X.; Duan, Y.-Y.; Wang, X.-D. Vapor−Liquid Equilibria Predictions for New Refrigerant Mixtures Based on Group Contribution Theory. *Ind. Eng. Chem. Res.* **2007**, *46*, 9274–9284.
(37) Hirata, Y.; Shimonosono, T. Mixing Rules of Young's Modulus, Thermal Expansion Coefficient and Thermal Conductivity of Solid Material with Particulate Inclusion. *J. Korean Ceram. Soc.* **2016**, *53*, 43–49.
(38) Kim, B.; Choi, S. H.; Zhu, X.-Y.; Frisbie, C. D. Molecular Tunnel Junctions Based on π-Conjugated Oligoacene Thiols and Dithiols between Ag, Au, and Pt Contacts: Effect of Surface Linking Group and Metal Work Function. *J. Am. Chem. Soc.* **2011**, *133*, 19864–19877.
(39) Beebe, J. M.; Engelkes, V. B.; Miller, L. L.; Frisbie, C. D. Contact Resistance in Metal−Molecule−Metal Junctions Based on Aliphatic SAMs: Effects of Surface Linker and Metal Work Function. *J. Am. Chem. Soc.* **2002**, *124*, 11268–11269.
(40) Engelkes, V. B.; Beebe, J. M.; Frisbie, C. D. Length-Dependent Transport in Molecular Junctions Based on SAMs of Alkanethiols and Alkanedithiols: Effect of Metal Work Function and Applied Bias on Tunneling Efficiency and Contact Resistance. *J. Am. Chem. Soc.* **2004**, *126*, 14287–14296.
(41) Xie, Z.; Bâldea, I.; Frisbie, C. D. Determination of Energy-Level Alignment in Molecular Tunnel Junctions by Transport and Spectroscopy: Self-Consistency for the Case of Oligophenylene Thiols and Dithiols on Ag, Au, and Pt Electrodes. *J. Am. Chem. Soc.* **2019**, *141*, 3670–3681.
(42) Xie, Z.; Bâldea, I.; Frisbie, C. D. Energy Level Alignment in Molecular Tunnel Junctions by Transport and Spectroscopy: Self-Consistency for the Case of Alkyl Thiols and Dithiols on Ag, Au, and Pt Electrodes. *J. Am. Chem. Soc.* **2019**, *141*, 18182–18192.
(43) Bâldea, I. Estimating the Number of Molecules in Molecular Junctions Merely Based on the Low Bias Tunneling Conductance at Variable Temperature. *IJMS* **2022**, *23*, 14985.
(44) Bâldea, I. Can Tunneling Current in Molecular Junctions Be so Strongly Temperature Dependent to Challenge a Hopping Mechanism? Analytical Formulas Answer This Question and Provide Important Insight into Large Area Junctions. *Phys. Chem. Chem. Phys.* **2024**, *26*, 6540–6556.
(45) Demissie, A. T.; Haugstad, G.; Frisbie, C. D. Quantitative Surface Coverage Measurements of Self-Assembled Monolayers by Nuclear Reaction Analysis of Carbon-12. *J. Phys. Chem. Lett.* **2016**, *7*, 3477–3481.
(46) Chen, Y.; Bâldea, I.; Yu, Y.; Liang, Z.; Li, M.-D.; Koren, E.; Xie, Z. CP-AFM Molecular Tunnel Junctions with Alkyl Backbones Anchored Using Alkynyl and Thiol Groups: Microscopically Different Despite Phenomenological Similarity. *Langmuir* **2024**, *40*, 4410–4423.

(47) Cederbaum, L. S. One-Body Green's Function for Atoms and Molecules: Theory and Application. *J. Phys. B: At. Mol. Phys.* **1975**, *8*, 290−303.
(48) von Niessen, W.; Schirmer, J.; Cederbaum, L.S. Computational Methods for the One-Particle Green's Function. *Comput. Phys. Rep.* **1984**, *1*, 57−125.
(49) Xie, Z.; Bâldea, I.; Frisbie, C. D. Why one can expect large rectification in molecular junctions based on alkane monothiols and why rectification is so modest. *Chem. Sci.* **2018**, *9*, 4456-4467.
(50) Xie, Z.; Bâldea, I.; Nguyen, Q.; Frisbie, C. D. Quantitative Analysis of Weak Current Rectification in Molecular Tunnel Junctions Subject to Mechanical Deformation Reveals Two Different Rectification Mechanisms for Oligophenylene Thiols versus Alkane Thiols. *Nanoscale* **2021**, *13*, 16755−16768.
(51) Bâldea, I. A Quantum Chemical Study from a Molecular Perspective: Ionization and Electron Attachment Energies for Species Often Used to Fabricate Single-Molecule Junctions. *Faraday Discuss.* **2014**, *174*, 37–56.
(52) Bâldea, I. Quantifying the relative molecular orbital alignment for molecular junctions with similar chemical linkage to electrodes. *Nanotechnology.* **2014**, *25*, 455202.
(53) Frisch, M. J.; Trucks, G. W.; Schlegel, H. B.; Scuseria, G. E.; Robb, M. A.; Cheeseman, J. R.; Scalmani, G.; Barone, V.; Petersson, G. A.; Nakatsuji, H.; Li, X.; Caricato, M.; Marenich, A. V.; Bloino, J.; Janesko, B. G.; Gomperts, R.; Mennucci, B.; Hratchian, H. P.; Ortiz, J. V.; Izmaylov, A. F.; Sonnenberg, J. L.; Williams-Young, D.; Ding, F.; Lipparini, F.; Egidi, F.; Goings, J.; Peng, B.; Petrone, A.; Henderson, T.; Ranasinghe, D.; Zakrzewski, V. G.; Gao, J.; Rega, N.; Zheng, G.; Liang, W.; Hada, M.; Ehara, M.; Toyota, K.; Fukuda, R.; Hasegawa, J.; Ishida, M.; Nakajima, T.; Honda, Y.; Kitao, O.; Nakai, H.; Vreven, T.; Throssell, K.; Montgomery, J. A., Jr.; Peralta, J. E.; Ogliaro, F.; Bearpark, M. J.; Heyd, J. J.; Brothers, E. N.; Kudin, K. N.; Staroverov, V. N.; Keith, T. A.; Kobayashi, R.; Normand, J.; Raghavachari, K.; Rendell, A. P.; Burant, J. C.; Iyengar, S. S.; Tomasi, J.; Cossi, M.; Millam, J. M.; Klene, M.; Adamo, C.; Cammi, R.; Ochterski, J. W.; Martin, R. L.; Morokuma, K.; Farkas, O.; Foresman, J. B.; Fox, D. J. Gaussian 16, Revision B.01; Gaussian, Inc.: Wallingford, CT, 2016.

TOC